

# Pressure-Enriched Chemistry of Pt: Prediction and Synthesis of Dense Sodium Platinides

HPSTAR  
 1319-2021

Jianjun Mao, Yida Wang, Kuo Li,\* and Yue Chen\*



Cite This: *J. Phys. Chem. C* 2021, 125, 11791–11798



Read Online

ACCESS |



Metrics & More

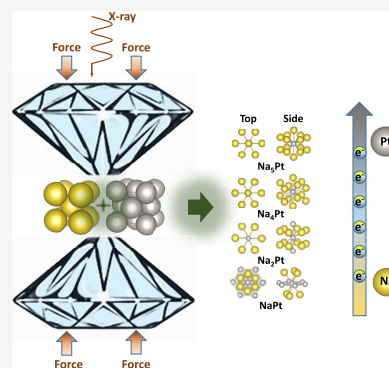


Article Recommendations



Supporting Information

**ABSTRACT:** Transition-metal anions, such as platinum (Pt) anions, are rare, and their unusual valence states may induce unique crystal topologies and novel properties. Although Pt anions have been reported, a high negative valence state of Pt and the route to obtain it have not been systematically studied. Herein, we report that high pressure can enrich the chemistry of Pt and result in various platinides through a reaction with sodium (Na). Using first-principles calculations in combination with an evolutionary algorithm, we discover several Na-rich platinides with unprecedented stoichiometries (e.g., Na<sub>2</sub>Pt, Na<sub>4</sub>Pt, and Na<sub>5</sub>Pt) and find that they adopt similar Pt–Na polyhedrons, where Pt can gain more than one electron donated by Na atoms. With the increase of the Na content, the ionicity of Pt becomes stronger. Frontier orbitals of Na<sub>4</sub>Pt and Na<sub>5</sub>Pt are not only dominated by Pt 5d orbitals, but also by Pt 6p orbitals. Furthermore, the predicted Na<sub>2</sub>Pt (space group: *P6/mmm*) and Na<sub>4</sub>Pt (space group: *I4/m*) are synthesized in a diamond anvil cell (DAC) and characterized by synchrotron X-ray diffraction at 4.5 GPa. The strong anisotropic properties of Na<sub>2</sub>Pt and the intriguing frontier orbitals of Na<sub>4</sub>Pt induced by Pt anions are further discussed.



## INTRODUCTION

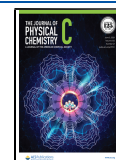
Platinum (Pt) is one of the least reactive and precious metals. Its ultrahigh malleability, strong corrosion-resistance, antioxidation at high temperatures, and structural stability under high pressures lead to widespread industrial applications.<sup>1–5</sup> However, under certain conditions, the chemistry of Pt can be greatly enriched, forming various compounds (halides, oxides, etc.).<sup>6,7</sup> The unusual relativistic effect is crucial in setting Pt and its compounds apart from other metals and their compounds.<sup>8,9</sup> The expansion of the 5d orbitals facilitates Pt to lose electrons in these compounds and presents the most common +2 and +4 valence states.<sup>6,7</sup> The rare +1 and +3 valence states are observed in bimetallic or polymetallic materials, stabilized by metal bonding.<sup>10</sup> Also, an unexpected +6 valence state of Pt was discovered in PtF<sub>6</sub>, which is one of the strongest oxidizers, playing a critical role in the discovery of the first noble gas compound XePtF<sub>6</sub>.<sup>11</sup> In contrast, the distinct contraction of the 6s shell structure makes Pt one of the most prominent transition metals with unconventional properties,<sup>9,12</sup> as reflected by its high electron affinity of 2.13 eV, which surpasses the values of chalcogens (S: 2.08 eV) and approaches the values of halogens (I: 3.06 eV).<sup>13</sup> In addition, the electronegativity of Pt (Pauling scale: 2.2) is only slightly lower than that of iodine (2.66). All these features indicate that Pt can exhibit negative valence states. Previously, the limits to valence states in transition metals have been deliberated by Riedel et al.<sup>14,15</sup> In contrast to the late main group elements, transition metals are rarely found to form anions and show negative valence states.

According to Miedema's rules,<sup>16</sup> small differences in electron charge density and large differences in electronegativity (or work function) between two metals are conducive to the formation of compounds. Therefore, alkali metals, alkali earth metals, and rare earth metals may form intermetallics consisting of negatively charged platinum ions, which have attracted considerable research interest.<sup>17,18</sup> In addition to gold, which may lead to a transition-metal anion,<sup>19</sup> cesium platinide Cs<sub>2</sub>Pt, a dark red transparent crystalline compound that adopts the Ni<sub>2</sub>In-type structure synthesized at a high temperature,<sup>20</sup> was found to contain a Pt<sup>2–</sup> anion.<sup>8</sup> Several barium platinides have also been obtained, in which Pt exhibits negative valence states ranging from –1 to –2.<sup>21</sup> These platinides include BaPt, Ba<sub>3</sub>Pt<sub>2</sub>, and Ba<sub>2</sub>Pt, which show a mix of ionic and metallic characteristics due to the higher electronegativity of Ba compared to Cs. The highest negative valence state of Pt discovered so far is equal to –3, reported in La<sub>2</sub>Pt<sub>2</sub>In<sup>22</sup> as a dimeric anion [Pt–Pt]<sup>–6</sup>. Besides, Pt can also show a negative valence state at electrochemically reduced surfaces.<sup>23</sup> These negative valence states of Pt are nontrivial for a metallic element and may induce extraordinary properties. Some of the compounds are considered to extend the Zintl–

Received: April 29, 2021

Revised: May 13, 2021

Published: May 24, 2021



Klemm concept to transition metals.<sup>24</sup> The hexagonally ordered linear chains of Pt anions forming stacked two-dimensional (2D) sheets in BaPt and Li<sub>2</sub>Pt can lead to a Dirac point at *K* point similar to graphene; such a phenomenon may shed light on the design of three-dimensional Dirac semimetals (DSMs).<sup>25</sup>

High pressure has emerged as a widely explored approach to synthesize compounds with atypical stoichiometries and unusual properties, such as the interstitial quasiatoms (ISQs) in electrides.<sup>26</sup> High pressure can also push the limits of the maximally reachable valence states of atoms, leading to new chemistry by activating elements' core electrons or unoccupied orbitals.<sup>27</sup> For instance, the inner shell of Cs can become reactive under high pressures, acting as a *p*-block element.<sup>28</sup> Recently, Yang et al. predicted theoretically that gold may also act as a 6*p* element in Li-rich aurides at high pressures.<sup>29</sup> These findings greatly benefited from the developments of first-principles prediction methods and DAC techniques.

The chemical reactivity of alkali metals experiences a large variation under pressures with subshell electronic transitions;<sup>30</sup> e.g., Na becomes the most electropositive *s*<sup>1</sup> element under pressure.<sup>31</sup> At 200 GPa, Na was reported to crystallize in a Ni<sub>2</sub>In-type phase (space group: *P*6<sub>3</sub>/*mmc*), whose Na atoms occupy the Ni sites and the ISQs occupy the In sites.<sup>32</sup> Furthermore, Na readily forms a fluorite-type compound with Helium (He) at experimentally accessible pressures,<sup>33</sup> which is different from the "hot" high-pressure van der Waals He-related compounds (e.g., NH<sub>3</sub>-He).<sup>34</sup> In addition to NaCl, unexpected stoichiometry compounds such as NaCl<sub>7</sub>, NaCl<sub>3</sub>, Na<sub>3</sub>Cl<sub>2</sub>, Na<sub>2</sub>Cl, and Na<sub>3</sub>Cl<sup>35</sup> become stable under high pressures. At ambient pressure, LiPt<sub>7</sub>, LiPt<sub>2</sub>, LiPt, and Li<sub>2</sub>Pt can be obtained at high temperatures.<sup>36–38</sup> Among these compounds, Li<sub>2</sub>Pt is known to exist at a normal atmosphere, which is formed by reacting LiH and Pt at 870 K,<sup>36</sup> while pressure can drive its formation at room temperature.<sup>39</sup> Therefore, there is a prospect for the formation of unusual stoichiometric sodium platinides by virtue of pressure. NaPt<sub>2</sub> is the only compound known in the Na–Pt binary system at ambient conditions.<sup>37,40</sup> Because Pt is widely used as an electrode for conductivity measurement of Na and the related compounds under high pressures,<sup>41,42</sup> the possible reactions between them are of practical importance.

Herein, we conduct an extensive structural investigation on stable Na–Pt compounds under high pressures (0–20 GPa) using the evolutionary theory based on first-principles calculations and the experimental DAC technique. In addition to the known NaPt<sub>2</sub> compound, unusual Na-rich stoichiometric Na<sub>2</sub>Pt, Na<sub>4</sub>Pt, and Na<sub>5</sub>Pt are found to be stable. Despite the wide range of stoichiometries, some of them crystallize in the same space group or consist of similar Pt–Na polyhedrons as building blocks. In the Na-rich platinides, a Pt atom is predicted to receive more than one electron from Na and has a valence state below  $-1$ . In our DAC experiment, Na<sub>2</sub>Pt and a tetragonal phase of Na<sub>4</sub>Pt are successfully synthesized. The unparalleled features of the platinides further extend our understanding of the rich chemistry of Pt under high pressures.

## MODEL AND METHODS

**Theoretical Calculations.** We first carried out a crystal structure search with variable compositions using USPEX.<sup>43</sup> The pressures were set to 0, 5, 10, 15, and 20 GPa with a maximum of 32 atoms; at each pressure, three structural searches were performed for atomic numbers in the ranges of

4–8, 8–16, and 16–32. We also performed structural searches with fixed compositions based on the results of the variable composition search. The evolutionary algorithm<sup>44</sup> applied in this work can be used to search for the lowest-enthalpy structures at a given pressure and to predict stable compounds and crystal structures given just the chemical elements involved. This method has been successfully applied to predict the structures for many systems with results confirmed by experiments.<sup>33,35,45–48</sup> Structural optimizations were performed based on density functional theory (DFT) with the Perdew–Burke–Ernzerhof (PBE) functional in the framework of the projector augmented wave (PAW) method,<sup>49</sup> as implemented in VASP.<sup>50</sup> 3*s*<sup>1</sup> and 5*d*<sup>9</sup>6*s*<sup>1</sup> were treated as the valence electrons of Na and Pt, respectively. A cutoff energy of 600 eV and Brillouin zone sampled with a resolution of around  $2\pi \times 0.03 \text{ \AA}^{-1}$  were used to ensure that the enthalpy calculations were converged within 1 meV per atom. Spin–orbit coupling (SOC) was considered for the calculations of the density of states and band structures.

The first generation of crystal structures was created randomly. All structures were relaxed at constant pressures and 0 K. The stability of different Na–Pt compounds with respect to the elemental Na and Pt solid bulk phases was evaluated through the enthalpy of formation

$$\Delta H_f(\text{Na}_x\text{Pt}_y) = [(x + y)H(\text{Na}_x\text{Pt}_y) - xH(\text{Na}) - yH(\text{Pt})]/(x + y)$$

where all enthalpies  $H = U + PV$  are given per atom;  $U$ ,  $P$ , and  $V$  are the internal energy, pressure, and volume, respectively. Based on the formation enthalpies, a convex hull can be constructed. The phases on the convex hull are thermodynamically stable. The energetically most unstable structures (40%) were discarded, and a new generation was created, 20% randomly and 80% from the lowest-enthalpy structures through heredity, lattice mutation, and soft mutation. To determine the dynamical stabilities of the predicted structures, phonon calculations were performed using the Phonopy code.<sup>51</sup> Bader charge analysis was performed to determine the charge transfer.<sup>52</sup> The crystal orbital Hamilton population (COHP) and the integrated COHP (ICOHP) were calculated using the LOBSTER program.<sup>53</sup>

**Experimental Procedures.** To provide further evidence for the predicted new compounds, in situ high-pressure synchrotron X-ray experiments were performed at the beamline 15U1 at the Shanghai Synchrotron Radiation Facility. A symmetric-style diamond anvil cell (DAC) with an anvil culet size of 400  $\mu\text{m}$  in diameter was used for applying pressure. A T301 stainless steel gasket was preindented to a thickness of  $\sim 30 \mu\text{m}$ , and a hole with a diameter of 180  $\mu\text{m}$  was drilled at the center of the preindented area as the sample chamber. To study the Na-rich compounds, a small sodium chip and 200 mesh platinum powder with a volume ratio of about 85:15 were coloaded into the sample chamber. The entire sample loading process was completed in an argon glovebox equipped with a microscope to prevent Na oxidation in air. The pressure was calibrated by Pt peak shift. The X-ray powder diffraction (XRD) pattern was integrated by Dioptas,<sup>54</sup> and the Le bail refinement of XRD data was conducted with Jana 2006<sup>55</sup> software.

## RESULTS AND DISCUSSION

**Energetics and Crystal Structures.** Extensive structural searches were performed to identify potentially stable Na–Pt compounds. The predicted phases with the lowest formation enthalpies for different compositions are used to construct the convex hulls under pressures. At 0 GPa as depicted in Figure 1,

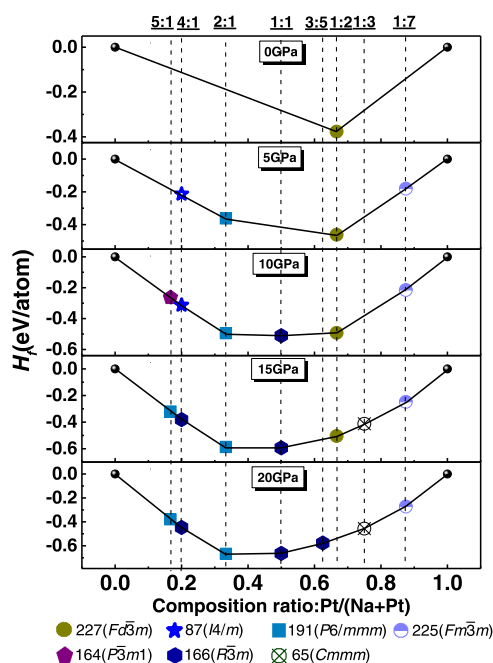


**Figure 1.** Convex hull diagram for the Na–Pt system with respect to Na and Pt at selected pressures. The body-centered cubic (bcc) phase of Na<sup>56</sup> and the face-centered cubic (fcc) phase of Pt<sup>5</sup> are used to evaluate the formation enthalpies. At 5 GPa, the hollow pentagram denotes the tetragonal Na<sub>4</sub>Pt (*I4/m*) that stays above but very close to the hull.

the already known stoichiometry NaPt<sub>2</sub> is readily identified in our calculation, validating the structure searching method and pseudopotentials applied to the Na–Pt system. Our predicted lattice parameter of NaPt<sub>2</sub> is 7.57 Å (prototype-type MgCu<sub>2</sub>, *Fd-3m* (227)), in agreement with the experimental result of 7.60 Å.<sup>37</sup> The Na-rich compounds Na<sub>2</sub>Pt, Na<sub>4</sub>Pt, and Na<sub>5</sub>Pt become energetically stable at 5, 10, and 10 GPa, respectively. NaPt becomes stable at around 10 GPa. Besides the already synthesized NaPt<sub>2</sub>, NaPt<sub>7</sub>, NaPt<sub>3</sub>, and Na<sub>3</sub>Pt<sub>5</sub> are new stable stoichiometries identified in the Pt-rich part. Phonon calculations indicate the dynamical stabilities of these compounds in the respective pressure ranges. Selected phonon dispersions are presented in Figures S1–S3. It is also noted that Na<sub>4</sub>Pt and Na<sub>5</sub>Pt are predicted to undergo structural phase transitions. The corresponding enthalpy differences of the competing phases as functions of pressures are shown in Figures S2 and S3. With the increase of pressure, Na<sub>4</sub>Pt transforms from the tetragonal *I4/m* phase, which is analogous to Li<sub>4</sub>Au,<sup>29</sup> to a rhombohedral *R-3m* phase at around 11 GPa. A soft-phonon-driven phase transition of Na<sub>5</sub>Pt from *P-3m1* to *P6/mmm* is predicted at approximately 10 GPa with Na displacing vertically along the *z*-axis (lattice direction *c*), as shown in Figure S3b.

Despite the different stoichiometries, some of the Na–Pt compounds tend to have the same spatial symmetry. Na<sub>2</sub>Pt adopts the MgB<sub>2</sub>-type structure (space group, *P6/mmm*)

throughout the pressure range investigated, analogous to Li<sub>2</sub>Pt.<sup>36,39</sup> It is seen from Figure 2a that Na atoms form a honeycomb layered sublattice in the *ab* plane, while Pt atoms form one-dimensional (1D) chains along the *c*-axis with equal Pt–Pt distance of 2.674 Å, which is close to the Pt–Pt bond length in Li<sub>2</sub>Pt<sup>39,57</sup> and is shorter than those in Pt bulk (2.756 Å) and NaPt<sub>3</sub> (2.700 Å) at 15 GPa. It is noted that Na<sub>5</sub>Pt may also crystallize in the same space group and the crystal structure can be obtained by alternately replacing the Pt layers in Na<sub>2</sub>Pt with Na, as shown in Figure 2b. For Na<sub>3</sub>Pt<sub>5</sub>, NaPt, and Na<sub>4</sub>Pt, they all adopt the *R-3m* space group. NaPt contains alternating Na and Pt layers along the *c* direction. NaPt<sub>7</sub> is analogous to a 2 × 2 × 2 Pt superlattice, crystallizing in the *Fm-3m* space group, with part of the Pt atoms replaced by Na forming an fcc sublattice, which is similar to the previously reported LiPt<sub>7</sub>.<sup>38</sup> To compare the structural variations of the different stoichiometries, we summarize the shortest Na–Pt, Na–Na, and Pt–Pt distances of Na–Pt compounds at 15 GPa in Figure S4. Increasing Na content does not significantly vary the Na–Pt distance; however, it enlarges the separation between the two nearest Pt atoms (Figure S4), making them more isolated in Na<sub>4</sub>Pt and Na<sub>5</sub>Pt.

To better understand the crystal structures of the Na-rich compounds, radial distribution functions (RDFs) *g(r)* with Pt as the reference atom at 15 GPa are given in Figure 3. Polyhedrons that consist of the first and second coordination shells of NaPt, Na<sub>2</sub>Pt, and Na<sub>5</sub>Pt are illustrated in the insets of Figure 3a,b, and d, respectively. For Na<sub>4</sub>Pt, the corresponding polyhedron that consists of the first three shells is given in the inset of Figure 3c. Most of these shells tend to form a honeycomb spatial arrangement along the *c*-axis as depicted in Figure S5. Na<sub>2</sub>Pt, Na<sub>4</sub>Pt, and Na<sub>5</sub>Pt have similar coordination polyhedrons and a coordination number of 14. The Pt atom in Na<sub>2</sub>Pt is coordinated by 12 Na atoms and 2 Pt atoms, forming a Pt chain and stacked hexagonal Na sheets. In Na<sub>4</sub>Pt and Na<sub>5</sub>Pt, Pt is coordinated by Na only. The minor difference between the buckled and planer Na honeycomb sheets in Na<sub>4</sub>Pt and Na<sub>5</sub>Pt is denoted by the red triangles in the insets of Figure 3c,d. With the increase of the Na content, the dimensionality of the Pt complex gradually reduces from the 2D Pt layer in NaPt through the 1D chain in Na<sub>2</sub>Pt to a zero-dimensional (0D) Pt atom in Na<sub>4</sub>Pt and Na<sub>5</sub>Pt. The hypercoordination observed in the predicted Na-rich compounds also suggests hypervalence,<sup>27</sup> which will be further discussed in the following sections.

**Electronic Structure and Chemical Bonding.** Bader charge analysis is performed to illustrate the charge transfer between Na and Pt, by partitioning the space into Bader basins around each atom based on stationary points in the charge density.<sup>52</sup> Integration of the charges in each basin gives the total charge associated with each atom. Pressure and different Wyckoff sites generally do not have a strong effect on the transferred charge between Na and Pt in most of these compounds, as shown in Figure S6. The average charge-transfer per atom at 15 GPa is illustrated in Figure 4a to show the ionization of Pt, which may also be visualized by the charge density difference (CDD) (crystal charge density minus superposition of isolated atomic charge densities) as shown in Figure S7a–d. We observe from Figure 4a that the Bader charge of Na is less sensitive to chemical composition. On the other hand, the Bader charge of Pt increases largely with the increasing Na content, indicating that the ionization of Pt may be effectively modulated under high pressures.

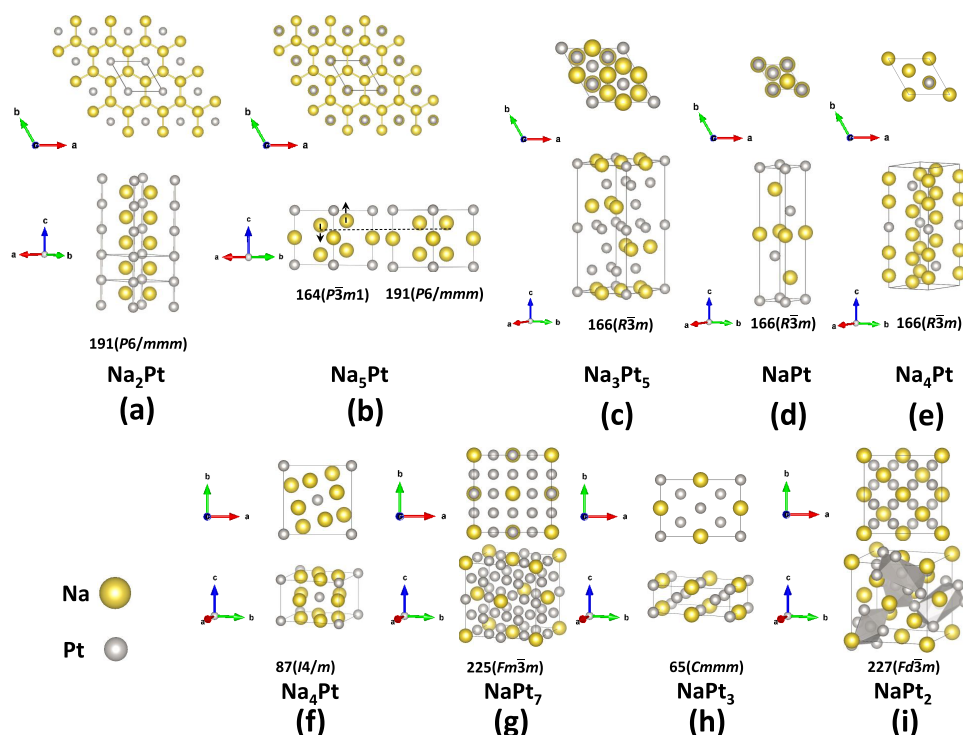


**Figure 2.** Predicted crystal structures of Na–Pt compounds under hydrostatic pressures. Their lattice parameters are summarized in Table S1 of the Supporting Information.

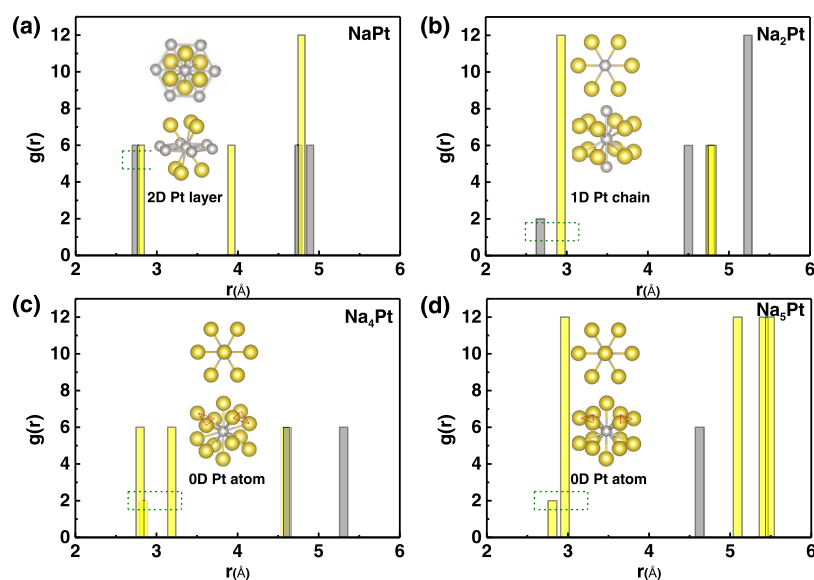


**Figure 3.** Radial distribution functions (RDFs)  $g(r)$  of NaPt (a),  $\text{Na}_2\text{Pt}$  (b),  $\text{Na}_4\text{Pt}$  (c), and  $\text{Na}_5\text{Pt}$  (d) at 15 GPa with Pt as the reference atom; yellow and gray bars denote Na and Pt atoms, respectively. Insets show the coordination polyhedrons around a Pt atom, corresponding to the neighboring atoms in dotted rectangles.

The charge transfer also contributes to the stabilization of the Na-rich platinides. Because the charge transfer from Na to Pt in  $\text{Na}_2\text{Pt}$ ,  $\text{Na}_4\text{Pt}$ , and  $\text{Na}_5\text{Pt}$  is high, a strong interaction between Na and Pt is expected, which can be directly probed by calculating the ICOHPs, as shown in Figure 4b. It is seen that the Pt–Pt bond has the highest strength. Pt anions in  $\text{Na}_4\text{Pt}$  and  $\text{Na}_5\text{Pt}$  are isolated in the Na matrix; thus, there is no Pt–Pt bond. In contrast, the interaction between Na and Na is the weakest. From the CDDs and the electron localization functions (ELFs) of NaPt,  $\text{Na}_2\text{Pt}$ ,  $\text{Na}_4\text{Pt}$ , and  $\text{Na}_5\text{Pt}$  shown in Figure S7, we observe that electrons are mainly around Pt and

the charge density between Na and Pt is low, suggesting ionic bonding features. On the other hand, the total densities of states of these compounds show a metallic character (see Figure S8). Considering that Bader charge analysis often underestimates the actual valence state,<sup>29,58</sup> Pt in  $\text{Na}_4\text{Pt}$  and  $\text{Na}_5\text{Pt}$  could have valence states below  $-2$ . Although it was reported that there is no direct relationship between static electronic charge and oxidation state,<sup>59</sup> using a machine learning algorithm and linear regression, Posysaev et al.<sup>58</sup> showed that a linear relationship exists between the oxidation state and the Bader charge for a large number of compounds.

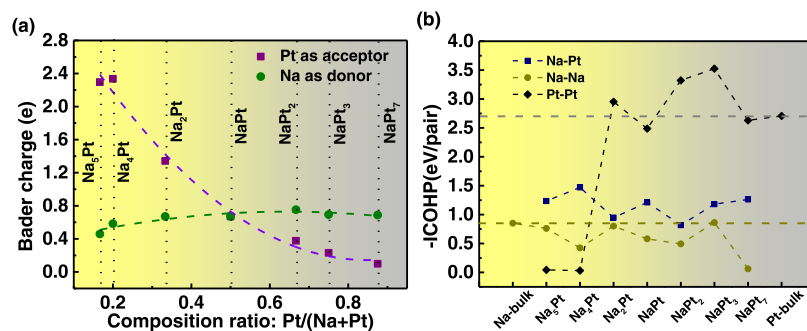


**Figure 4.** (a) Average Bader charge-transfer per atom in various Na–Pt compounds (absolute values are given) at 15 GPa. (b) Integrated crystal orbital Hamiltonian populations (ICOHPs) of atomic pairs with the shortest distances in different Na–Pt compounds; here, positive values represent bonding states. Dashed lines are guides to the eyes.

Nonetheless, the exact oxidation states of Pt in these platinumides need further experimental confirmation.

Electron configuration is crucial in explaining the chemical properties of elements, including reactivity and periodicity.<sup>60</sup> To further understand the nature of the frontier energy levels, we have also calculated the projected density of states (PDOSs) and band structures of Na-rich compounds at 15 GPa as depicted in Figures 5 and S9. The 5d orbitals of Pt in

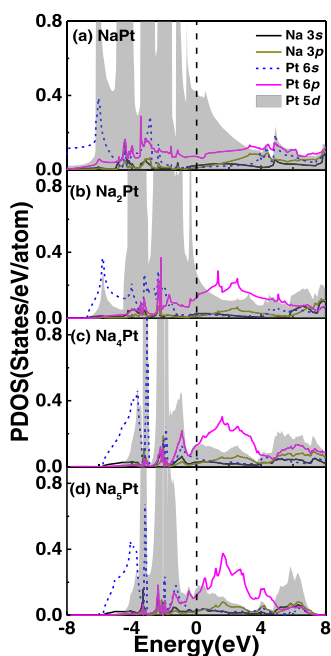


**Figure 5.** Projected density of states (PDOSs) of (a) NaPt, (b) Na<sub>2</sub>Pt, (c) Na<sub>4</sub>Pt (*R*3*m*), and (d) Na<sub>5</sub>Pt (*P*6/*m**m**m*) at 15 GPa. The Fermi level locates at 0 eV.

Na<sub>4</sub>Pt and Na<sub>5</sub>Pt are localized and close to 5d<sup>10</sup> as illustrated in Figure S8, exhibiting isolated atomic orbital characteristics similar to the 5d orbitals of Pt in Ba<sub>2</sub>Pt.<sup>31</sup> The PDOS around the Fermi level as depicted in Figure 5 shows that the contribution from Pt 5d orbitals becomes smaller compared to that from Pt 6p orbitals with the increase of the Na content. For Na<sub>4</sub>Pt and Na<sub>5</sub>Pt, the frontier orbitals are not only dominated by the Pt 5d orbitals but also by the Pt 6p orbitals, showing the characteristics of a 6p element. This is in agreement with our analysis above that Pt shows high negative valence states in Na<sub>4</sub>Pt and Na<sub>5</sub>Pt. Taking Na<sub>4</sub>Pt as an example, where the Pt–Pt distance is large, we have

constructed a hypothetical model Na<sub>0</sub>Pt as shown in Figure S10, in which all Na atoms are removed from the Na<sub>4</sub>Pt lattice. The absence of 6p orbitals and the presence of partially filled 6s states suggest that Pt atoms accept electrons from Na. This hypothetical model also allows us to have an approximate comparison of the 6p orbitals of Pt in Na<sub>4</sub>Pt with those of Tl and Pb atoms in Na<sub>0</sub>Tl and Na<sub>0</sub>Pb (see Figure S10c,d).

**Experimental Synthesis of Na<sub>2</sub>Pt and Na<sub>4</sub>Pt under a High Pressure and Their Intriguing Properties.** To provide further evidence for the theoretical prediction of the new Na-rich Na–Pt compounds, we performed corresponding high-pressure experiments. The synchrotron XRD patterns at approximately 4.5 GPa at room temperature with Le Bail fitting are shown in Figure 6. It is seen that the XRD patterns

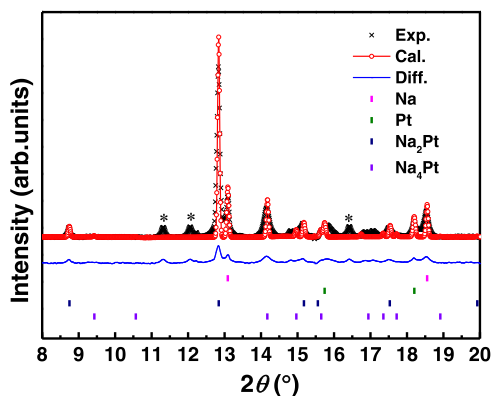


**Figure 6.** Synchrotron X-ray powder diffraction pattern and the Le Bail refinement plot ( $\lambda = 0.6199 \text{ \AA}$ ) of Na–Pt compounds at 4.5 GPa at room temperature. The black cross and red circle lines represent the experimental and the calculated data, respectively. The blue line shows the difference between the experimental and the calculated results. The pink, green, navy, and purple bars denote the contributions from Na, Pt, Na<sub>2</sub>Pt, and Na<sub>4</sub>Pt, respectively. The asterisks denote the unidentified reflections.

still contain peaks of unreacted Na and Pt, and the unidentified peaks in the XRD patterns may be attributed to the formation of unknown metastable phases. The refined lattice parameters from the XRD data are  $a = 4.695 \text{ \AA}$  and  $c = 2.773 \text{ \AA}$  for Na<sub>2</sub>Pt adopting a *P*6/*m**m**m* space group and  $a = 6.732 \text{ \AA}$  and  $c = 4.556 \text{ \AA}$  for Na<sub>4</sub>Pt adopting an *I*4/*m* space group. These experimental results are in agreement with our theoretical predictions. The theoretical lattice parameters are  $a = 4.721 \text{ \AA}$  and  $c = 2.750 \text{ \AA}$  for Na<sub>2</sub>Pt and  $a = 6.717 \text{ \AA}$  and  $c = 4.564 \text{ \AA}$  for Na<sub>4</sub>Pt at 4.5 GPa. Although Na<sub>4</sub>Pt is predicted to become

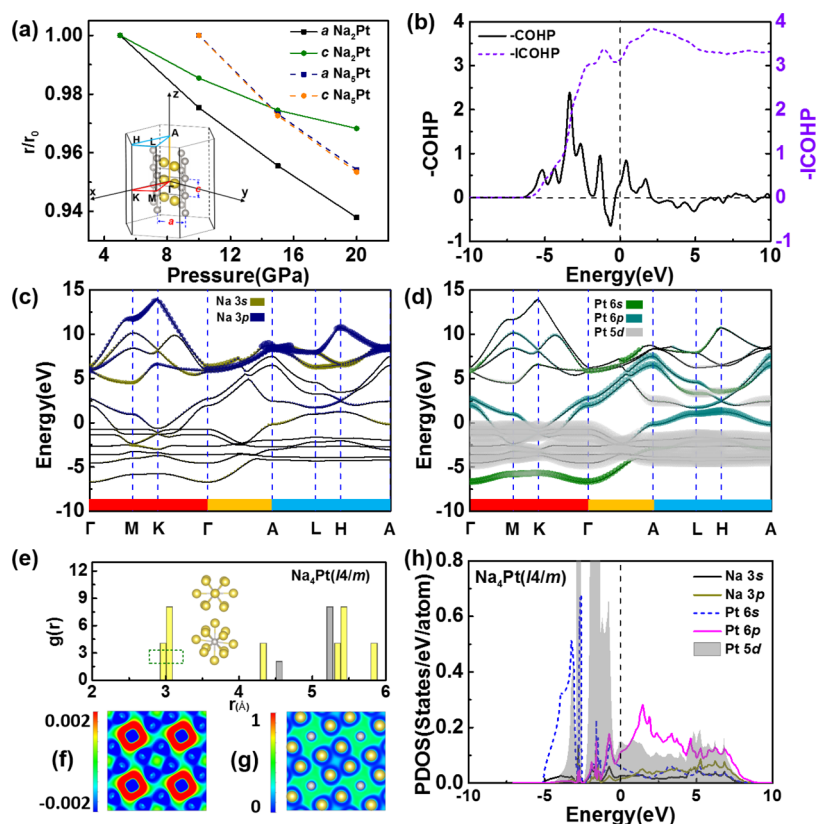


**Figure 7.** (a) Normalized lattice parameters of  $\text{Na}_2\text{Pt}$  and  $\text{Na}_4\text{Pt}$  as a function of pressure. (b) Negative COHP of the Pt–Pt bond in parallel to the lattice direction  $c$  (see inset in (a)) and its integral; the Fermi level is located at 0 eV. The projected band structure of  $\text{Na}_2\text{Pt}$  on Na (c) and Pt (d) at 5 GPa; widths of the bands show the contribution. Inset in (a) shows the Brillouin zone of  $\text{Na}_2\text{Pt}$  with specific  $k$  points considered in the band structure calculation. (e) RDF  $g(r)$  with Pt as the reference atom (yellow and gray bars refer to Na and Pt neighboring atoms, respectively), (f) CDD (in  $\text{e}/\text{\AA}^3$ ), (g) ELF, and (h) PDOS of  $I4/m$   $\text{Na}_4\text{Pt}$  at 5 GPa.

energetically stable between 5 and 10 GPa from DFT (see Figure 1), the actual stabilizing pressure may be affected by factors such as the exchange–correlation energy functional and experimental temperature.

$\text{Na}_2\text{Pt}$  and  $\text{Na}_4\text{Pt}$ , where Pt exhibits negative valence states, have intriguing properties. As shown in Figure 7a,  $\text{Na}_2\text{Pt}$  shows highly anisotropic compressibility. We find that  $a$  reduces by  $0.292 \text{ \AA}$  ( $-6.2\%$ ) when pressure is increased from 5 to 20 GPa. In contrast,  $c$  reduces by only  $0.087 \text{ \AA}$  ( $-3.1\%$ ). For comparison,  $\text{Na}_5\text{Pt}$ , which crystallizes in the same space group as  $\text{Na}_2\text{Pt}$ , has a much more isotropic compressibility. The highly anisotropic compressibility of  $\text{Na}_2\text{Pt}$  can be ascribed to the short Pt–Pt bonds along the lattice direction  $c$  penetrating the honeycomb Na sublattice. The strong interaction between these Pt atoms can also be revealed from the COHP as illustrated in Figure 7b. There is a large bonding contribution below the Fermi level and only a small antibonding contribution from  $-1.1$  to  $-0.5$  eV. Furthermore, analyzing the projected fat band structure along the specific Brillouin paths provides a deeper understanding of the bonding in  $\text{Na}_2\text{Pt}$ . As shown in Figure 7c,d, the bands associated with Pt 5d orbitals along paths vertical to the  $\Gamma$ –A direction are rather flat, while those parallel to this direction are more dispersive, suggesting a strong Pt–Pt interaction along the lattice direction  $c$ . Similar linear ordering of Pt atoms can also be found in other compounds such as  $\text{Li}_2\text{Pt}$  and  $\text{BaPt}$ .<sup>25</sup>

For the newly synthesized tetragonal  $\text{Na}_4\text{Pt}$  ( $I4/m$ ), the coordination polyhedron around a Pt atom is shown in Figure 7e. Compared to the coordination polyhedron of the high-

pressure rhombohedral ( $R\bar{3}m$ ) phase of  $\text{Na}_4\text{Pt}$  as depicted in the insets of Figure 3c, pressure increases the coordination number by 2. Electrons transfer from Na to Pt and accumulate around Pt atoms as illustrated in Figure 7f, leading to a high negative valence state of Pt with a Bader charge of  $-2.37$  e. The ELF, as shown in Figure 7g, is also similar to those of other Na-rich compounds, with mostly free electrons between Na and Pt. The energies of the valence atomic orbitals of Pt in  $I4/m$   $\text{Na}_4\text{Pt}$ , as shown in Figure 7h, increase in the order from 6s through 5d to 6p. A pronounced 6p component is observed around the Fermi level similar to the high-pressure  $R\bar{3}m$  phase.

## CONCLUSIONS

In summary, an evolutionary structure searching algorithm was combined with DFT energy calculations to explore the stabilities and crystal structures of Na–Pt compounds under high pressures. We find that various Na–Pt platinides with unexpected stoichiometries can form in an experimentally accessible pressure range. The crystal structures of some of these platinides are found to have similar building blocks. In the Na-rich platinides, Pt presents negative valence states and gains more electrons as the Na content increases. The electronic states in  $\text{Na}_4\text{Pt}$  and  $\text{Na}_5\text{Pt}$  around the Fermi level are described by Pt 5d and 6p orbitals.  $\text{Na}_2\text{Pt}$  and  $\text{Na}_4\text{Pt}$  are successfully synthesized in a DAC experiment at around 4.5 GPa. From synchrotron X-ray diffraction, the space groups and the lattice constants are determined, which agree with our theoretical results. The intriguing properties of  $\text{Na}_2\text{Pt}$  and  $\text{Na}_4\text{Pt}$  have also been further studied.

## ■ ASSOCIATED CONTENT

## SI Supporting Information

The Supporting Information is available free of charge at <https://pubs.acs.org/doi/10.1021/acs.jpcc.1c03836>.

Lattice parameters; phonon dispersions; enthalpy differences between competing phases; shortest atomic distances at 15 GPa; coordination shells; Bader charge transfer; CDD; ELF; TDOS; PDOS; and projected band structures (PDF)

## ■ AUTHOR INFORMATION

## Corresponding Authors

**Kuo Li** – Center for High Pressure Science and Technology Advanced Research, Beijing 100094, China; [orcid.org/0000-0002-4859-6099](https://orcid.org/0000-0002-4859-6099); Email: [likuo@hpstar.ac.cn](mailto:likuo@hpstar.ac.cn)

**Yue Chen** – Department of Mechanical Engineering, The University of Hong Kong, Hong Kong SAR, China; HKU Zhejiang Institute of Research and Innovation, Lin An 311305, China; [orcid.org/0000-0001-5811-6936](https://orcid.org/0000-0001-5811-6936); Email: [yuechen@hku.hk](mailto:yuechen@hku.hk)

## Authors

**Jianjun Mao** – Department of Mechanical Engineering, The University of Hong Kong, Hong Kong SAR, China; [orcid.org/0000-0003-2265-9685](https://orcid.org/0000-0003-2265-9685)

**Yida Wang** – Center for High Pressure Science and Technology Advanced Research, Beijing 100094, China

Complete contact information is available at: <https://pubs.acs.org/doi/10.1021/acs.jpcc.1c03836>

## Notes

The authors declare no competing financial interest.

## ■ ACKNOWLEDGMENTS

This work was supported by the National Natural Science Foundation of China (11874313), the Zhejiang Provincial Natural Science Foundation (LR19A040001), and the Research Grants Council of Hong Kong (17300018 and 17201019). The authors are grateful for the research computing facilities offered by ITS, HKU.

## ■ REFERENCES

- (1) McNaught, A. D.; Wilkinson, A. *Compendium of Chemical Terminology*; IUPAC Recommendations, 1997.
- (2) Rosenberg, B.; Van Camp, L.; Krigas, T. Inhibition of Cell Division in *Escherichia coli* by Electrolysis Products from a Platinum Electrode. *Nature* **1965**, *205*, 698–699.
- (3) Kelland, L. The Resurgence of Platinum-Based Cancer Chemotherapy. *Nat. Rev. Cancer* **2007**, *7*, 573–584.
- (4) Craig, B. D.; Anderson, D. S. *Handbook of Corrosion Data*; ASM International, 1994.
- (5) Holmes, N. C.; Moriarty, J. A.; Gathers, G. R.; Nellis, W. J. The Equation of State of Platinum to 660 GPa (6.6 Mbar). *J. Appl. Phys.* **1989**, *66*, 2962–2967.
- (6) Schweizer, A. E.; Kerr, G. T. Thermal Decomposition of Hexachloroplatinic Acid. *Inorg. Chem.* **1978**, *17*, 2326–2327.
- (7) Arnold, W.; Eric, S. P.; John, A. R.; Emory, E. T. Handbook of Organic Compounds. *Nature* **1956**, *177*, 639–640. DOI: 10.1038/177639a0.
- (8) Jansen, M. Effects of Relativistic Motion of Electrons on the Chemistry of Gold and Platinum. *Solid State Sci.* **2005**, *7*, 1464–1474.
- (9) Pyykko, P.; Desclaux, J. P. Relativity and the Periodic System of Elements. *Acc. Chem. Res.* **1979**, *12*, 276–281.

- (10) Kauffman, G. B.; Thurner, J. J.; Zatzko, D. A. Ammonium Hexachloroplatinate (IV). *Inorg. Synth.* **1967**, *9*, 182–185.

- (11) Bartlett, N. *Xenon Hexafluoroplatinate (V) Xe<sup>+</sup>[PtF<sub>6</sub>]*; Royal Soc Chemistry Thomas Graham House: Sciencepark, Milton Rd, Cambridge, 1962; 218.

- (12) Desclaux, J. P. Relativistic Dirac-Fock expectation values for atoms with  $Z = 1$  to  $Z = 120$ . *At. Data Nucl. Data Tables* **1973**, *12*, 311–406.

- (13) Andersen, T.; Haugen, H. K.; Hotop, H. Binding Energies in Atomic Negative Ions. III. *J. Phys. Chem. Ref. Data* **1999**, *28*, 1511–1533.

- (14) Groult, H.; Leroux, F.; Tressaud, A., *Modern Synthesis Processes and Reactivity of Fluorinated Compounds: Progress in Fluorine Science*; Elsevier, 2016.

- (15) Hu, S.-X.; Li, W.-L.; Lu, J.-B.; Bao, J. L.; Yu, H. S.; Truhlar, D. G.; Gibson, J. K.; Marçalo, J.; Zhou, M.; Riedel, S.; et al. On the Upper Limits of Oxidation States in Chemistry. *Angew. Chem., Int. Ed.* **2018**, *57*, 3242–3245.

- (16) Miedema, A. R.; De Boer, F. R.; De Chatel, P. F. Empirical Description of the Role of Electronegativity in Alloy Formation. *J. Phys. F: Met. Phys.* **1973**, *3*, No. 1558.

- (17) Kienast, G.; Verma, J.; Klemm, W. Das Verhalten Der Alkalimetalle Zu Kupfer, Silber Und Gold. *Z. Anorg. Allg. Chem.* **1961**, *310*, 143–169.

- (18) Karpov, A.; Jansen, M. A New Family of Binary Layered Compounds of Platinum with Alkali Metals (A = K, Rb, Cs). *Z. Anorg. Allg. Chem.* **2006**, *632*, 84–90.

- (19) Sommer, A. Alloys of Gold with Alkali Metals. *Nature* **1943**, *152*, 215.

- (20) Karpov, A.; Nuss, J.; Wedig, U.; Jansen, M. Cs<sub>2</sub>Pt: A Platinum (-II) Exhibiting Complete Charge Separation. *Angew. Chem., Int. Ed.* **2003**, *42*, 4818–4821.

- (21) Karpov, A.; Konuma, M.; Jansen, M. An Experimental Proof for Negative Oxidation States of Platinum: ESCA-Measurements on Barium Platinides. *Chem. Commun.* **2006**, 838–840.

- (22) Köhler, J.; Whangbo, M. H. Late Transition Metal Anions Acting as *p*-Metal Elements. *Solid State Sci.* **2008**, *10*, 444–449.

- (23) Ghilane, J.; Lagrost, C.; Guilloux-Viry, M.; Simonet, J.; Delamar, M.; Mangeney, C.; Hapiot, P. Spectroscopic Evidence of Platinum Negative Oxidation States at Electrochemically Reduced Surfaces. *J. Phys. Chem. C* **2007**, *111*, 5701–5707.

- (24) Karpov, A.; Nuss, J.; Wedig, U.; Jansen, M. Covalently Bonded [Pt]<sup>-</sup> Chains in BaPt: Extension of the Zintl-Klemm Concept to Anionic Transition Metals? *J. Am. Chem. Soc.* **2004**, *126*, 14123–14128.

- (25) Gibson, Q. D.; Schoop, L. M.; Muechler, L.; Xie, L.; Hirschberger, M.; Ong, N. P.; Car, R.; Cava, R. J. Three-Dimensional Dirac Semimetals: Design Principles and Predictions of New Materials. *Phys. Rev. B* **2015**, *91*, No. 205128.

- (26) Miao, M.-S.; Hoffmann, R. High-Pressure Electrides: The Chemical Nature of Interstitial Quasiparticles. *J. Am. Chem. Soc.* **2015**, *137*, 3631–3637.

- (27) Miao, M. S.; Sun, Y.; Zurek, E.; Lin, H. Chemistry under High Pressure. *Nat. Rev. Chem.* **2020**, *4*, 508–527.

- (28) Miao, M.-S. Caesium in High Oxidation States and as a *p*-Block Element. *Nat. Chem.* **2013**, *5*, 846–852.

- (29) Yang, G.; Wang, Y.; Peng, F.; Bergara, A.; Ma, Y. Gold as a *6p*-Element in Dense Lithium Aurides. *J. Am. Chem. Soc.* **2016**, *138*, 4046–4052.

- (30) Rousseau, B.; Xie, Y.; Ma, Y.; Bergara, A. Exotic High Pressure Behavior of Light Alkali Metals, Lithium and Sodium. *Eur. Phys. J. B* **2011**, *81*, 1–14.

- (31) Rahm, M.; Cammi, R.; Ashcroft, N.; Hoffmann, R. Squeezing All Elements in the Periodic Table: Electron Configuration and Electronegativity of the Atoms under Compression. *J. Am. Chem. Soc.* **2019**, *141*, 10253–10271.

- (32) Ma, Y.; Eremets, M.; Oganov, A. R.; Xie, Y.; Trojan, I.; Medvedev, S.; Lyakhov, A. O.; Valle, M.; Prakapenka, V. Transparent Dense Sodium. *Nature* **2009**, *458*, 182–185.

- (33) Dong, X.; Oganov, A. R.; Goncharov, A. F.; Stavrou, E.; Lobanov, S.; Saleh, G.; Qian, G.-R.; Zhu, Q.; Gatti, C.; Deringer, V. L.; et al. A Stable Compound of Helium and Sodium at High Pressure. *Nat. Chem.* **2017**, *9*, 440–445.
- (34) Shi, J.; Cui, W.; Hao, J.; Xu, M.; Wang, X.; Li, Y. Formation of Ammonia-Helium Compounds at High Pressure. *Nat. Commun.* **2020**, *11*, No. 3164.
- (35) Zhang, W.; Oganov, A. R.; Goncharov, A. F.; Zhu, Q.; Boulfelfel, S. E.; Lyakhov, A. O.; Stavrou, E.; Somayazulu, M.; Prakapenka, V. B.; Konôpková, Z. Unexpected Stable Stoichiometries of Sodium Chlorides. *Science* **2013**, *342*, 1502–1505.
- (36) Bronger, W.; Nacken, B.; Ploog, K. Zur Synthese Und Struktur Von  $\text{Li}_2\text{Pt}$  Und  $\text{LiPt}$ . *J. Less-Common Met.* **1975**, *43*, 143–146.
- (37) Nash, C. P.; Boyden, F. M.; Whittig, L. D. Intermetallic Compounds of Alkali Metals with Platinum. A Novel Preparation of a Colloidal Platinum Hydrogenation Catalyst. *J. Am. Chem. Soc.* **1960**, *82*, 6203–6204.
- (38) Bronger, W.; Klessen, G.; Müller, P. Zur Struktur Von  $\text{LiPt}_7$ . *J. Less-Common Met.* **1985**, *109*, L1–L2.
- (39) Binns, J.; Marqués, M.; Dalladay-Simpson, P.; Turnbull, R.; Frost, M.; Gregoryanz, E.; Howie, R. T. Reactivity of Lithium and Platinum at Elevated Densities. *Phys. Rev. B* **2019**, *99*, No. 220101.
- (40) Range, K.-J.; Rau, F.; Klement, U. Sodium Diplatinum. *Acta Crystallogr., Sect. C* **1989**, *45*, 1069–1070.
- (41) Bridgman, P. W. Electrical Resistance under Pressure, Including Certain Liquid Metals. *Proc. Am. Acad. Arts Sci.* **1921**, *56*, 61–154.
- (42) Shimizu, K.; Kimura, T.; Furomoto, S.; Takeda, K.; Kontani, K.; Onuki, Y.; Amaya, K. Superconductivity in the Non-Magnetic State of Iron under Pressure. *Nature* **2001**, *412*, 316–318.
- (43) Lyakhov, A. O.; Oganov, A. R.; Valle, M. Crystal Structure Prediction Using Evolutionary Approach. *Mod. Methods Cryst. Struct. Predict.* **2010**, 147–180.
- (44) Oganov, A. R.; Lyakhov, A. O.; Valle, M. How Evolutionary Crystal Structure Prediction Works and Why. *Acc. Chem. Res.* **2011**, *44*, 227–237.
- (45) Chen, Y.; Hu, Q. M.; Yang, R. Predicted Suppression of the Superconducting Transition of New High-Pressure Yttrium Phases with Increasing Pressure from First-Principles Calculations. *Phys. Rev. Lett.* **2012**, *109*, No. 157004.
- (46) Yu, H.; Lao, W.; Wang, L.; Li, K.; Chen, Y. Pressure-Stabilized Tin Selenide Phase with an Unexpected Stoichiometry and a Predicted Superconducting State at Low Temperatures. *Phys. Rev. Lett.* **2017**, *118*, No. 137002.
- (47) Yu, H.; Lin, X.; Li, K.; Chen, Y. Unveiling a Novel, Cation-Rich Compound in a High-Pressure Pb–Te Binary System. *ACS Cent. Sci.* **2019**, *5*, 683–687.
- (48) Mao, J.; Chen, Y. Ground-State Crystal Structures of Superconducting  $\text{Nb}_3\text{Al}$  and the Phase Transformation under High Pressures. *J. Appl. Phys.* **2018**, *124*, No. 173902.
- (49) Blöchl, P. E. Projector Augmented-Wave Method. *Phys. Rev. B* **1994**, *50*, No. 17953.
- (50) Kresse, G.; Furthmüller, J. Efficiency of Ab-Initio Total Energy Calculations for Metals and Semiconductors Using a Plane-Wave Basis Set. *Comput. Mater. Sci.* **1996**, *6*, 15–50.
- (51) Togo, A.; Oba, F.; Tanaka, I. First-Principles Calculations of the Ferroelastic Transition between Rutile-Type and  $\text{CaCl}_2$ -Type  $\text{SiO}_2$  at High Pressures. *Phys. Rev. B* **2008**, *78*, No. 134106.
- (52) Henkelman, G.; Arnaldsson, A.; Jónsson, H. A Fast and Robust Algorithm for Bader Decomposition of Charge Density. *Comput. Mater. Sci.* **2006**, *36*, 354–360.
- (53) Dronskowski, R.; Blöchl, P. E. Crystal Orbital Hamilton Populations (COHP): Energy-Resolved Visualization of Chemical Bonding in Solids Based on Density-Functional Calculations. *J. Phys. Chem. A* **1993**, *97*, 8617–8624.
- (54) Prescher, C.; Prakapenka, V. B. Dioptas: A Program for Reduction of Two-Dimensional X-Ray Diffraction Data and Data Exploration. *High Pressure Res.* **2015**, *35*, 223–230.
- (55) Petříček, V.; Dušek, M.; Palatinus, L. Crystallographic Computing System Jana2006: General Features. *Z. Kristallogr. - Cryst. Mater.* **2014**, *229*, 345–352.
- (56) Hanfland, M.; Loa, I.; Syassen, K. Sodium under Pressure: *bcc* to *fcc* Structural Transition and Pressure-Volume Relation to 100 GPa. *Phys. Rev. B* **2002**, *65*, No. 184109.
- (57) Wu, G.; Wu, S.; Wu, P. Doping-Enhanced Lithium Diffusion in Lithium-Ion Batteries. *Phys. Rev. Lett.* **2011**, *107*, No. 118302.
- (58) Posyayev, S.; Miroshnichenko, O.; Alatalo, M.; Le, D.; Rahman, T. S. Oxidation States of Binary Oxides from Data Analytics of the Electronic Structure. *Comput. Mater. Sci.* **2019**, *161*, 403–414.
- (59) Jansen, M.; Wedig, U. A Piece of the Picture-Misunderstanding of Chemical Concepts. *Angew. Chem., Int. Ed.* **2008**, *47*, 10026–10029.
- (60) Pauling, L. *The Nature of the Chemical Bond*; Cornell University Press: Ithaca, NY, 1960; Vol. 260.